Effect of dislocations on the electrical and optical properties of long-wavelength infrared HgCdTe photovoltaic detectors

S. M. Johnson, D. R. Rhiger, J. P. Rosbeck, J. M. Peterson, S. M. Taylor, and M. E. Boyd
Santa Barbara Research Center, Goleta, California 93117

(Received 1 November 1991; accepted 9 April 1992)

The quantitative effects of dislocations on the electrical and optical properties of long-wavelength infrared (LWIR) HgCdTe photovoltaic detectors was determined by deliberately introducing dislocations into localized regions of two high-performance arrays having cutoff wavelengths of 9.5 and 10.3 μm at $T = 78$ K. Results show that dislocations can have a dramatic effect on detector R_0A product, particularly at temperatures below 78 K. For large dislocation densities, R_0A decreases as the square of the dislocation density; the onset of the square dependence occurs at progressively lower dislocation densities as the temperature decreases. A phenomenological model was developed which describes the dependence of the detector R_0A product with dislocation density, based on the conductances of individual and interacting dislocations which shunt the p–n junction. Spectral response and quantum efficiency are only weakly affected, as is the diffusion component of the leakage current. The $1/f$ noise current was found to increase approximately linearly with dislocation density and also tracks with the magnitude of the leakage current similar to a data trendline established for undamaged HgCdTe detectors. These results can be used to understand the performance limitations of LWIR HgCdTe arrays fabricated on heteroepitaxial substrates.

I. INTRODUCTION

Dislocations originating from material growth and array processing can affect the overall performance, uniformity, and operability of HgCdTe infrared focal plane arrays (IRFPAs). A quantitative understanding of the effect of dislocations on the electrical and optical properties of long-wavelength infrared (LWIR) HgCdTe photovoltaic (PV) detectors is needed to establish their role in determining overall array performance, uniformity, and operability. This is particularly important with regard to the growth of HgCdTe on heteroepitaxial Si-based and GaAs-based substrates, which have a higher dislocation density than the bulk CdZnTe substrates typically used for epitaxial HgCdTe materials growth.

The majority of earlier work done on the electrical properties of microstructural defects in HgCdTe was mostly focused on the effect of dislocations and subgrain boundaries on performance of metal–insulator semiconductor (MIS) detectors,[1–11] and on their effect on minority carrier lifetime.[12–15] Only more recently has any work been published on the effect of dislocations on HgCdTe PV detectors. It was found that an increased dislocation density in midwavelength infrared (MWIR) PV detectors, introduced by excess hybridization force, had a much more pronounced effect on excess g–r current than on excess diffusion current.[16]

The purpose of this work is to determine quantitatively the effect of dislocations on the electrical and optical properties of LWIR HgCdTe PV detectors, including current–voltage (I–V) characteristics versus temperature, spectral response, quantum efficiency, and $1/f$ noise. A detailed analysis of these properties was done on two different arrays which had cutoff wavelengths of 9.5 and 10.3 μm at $T = 78$ K. Additionally, a phenomenological model was developed which describes the dependence of the detector R_0A_j product (resistance at zero bias times junction area) with dislocation density, based on the conductances of individual and interacting dislocations which shunt the p–n junction.

II. EXPERIMENTAL TECHNIQUE

Our approach for determining the effect of dislocations on HgCdTe PV device properties was to induce dislocations by indenting localized regions of high-performance LWIR HgCdTe arrays. Using this approach, the effect of dislocations could be isolated from other bulk material, surface, and processing effects which can degrade device performance; these other mechanisms are already substantially reduced in high-performance arrays. Two different arrays were analyzed, Array 1 and Array 2, having cutoff wavelengths of 9.5 and 10.3 μm at $T = 78$ K, respectively. The cutoff wavelengths and junction areas of the detectors in these arrays are summarized in Table I. The p-on-n double-layer heterojunction backside-illuminated detectors were fabricated using intentionally doped HgCdTe layers grown by "infinite melt" vertical liquid phase epitaxy (LPE) from a Hg-rich solution on lattice-matched CdZnTe substrates.[17,18]

Dislocations were induced by indenting the arrays close to locations where diodes would be accessed by a fanout. Dislocations propagate outward from this indentation point into the diodes to be tested. The indentation was simply done using a modified tweezer tip with a slight pressure applied by hand. The dislocation density cannot be controlled, but only varied by changing the distance of the indentation location. Diodes that were analyzed were

 0734-211X/92/041499-08$01.00 ©1992 American Vacuum Society

Downloaded 26 Sep 2013 to 128.220.8.15. Redistribution subject to AVS license or copyright; see http://avspublications.org/jvstb/about/rights_and_permissions

TABLE I. Summary of the 78 K cutoff wavelengths and diode junction areas for Array 1 and Array 2.

Array	78 K cutoff wavelength (μm)	Junction area (cm^2)
Array 1	9.5	6.8×10^{-6}
Array 2	10.3	1.1×10^{-5}

several hundred microns away from the indentation point and no visible damage to these diodes was observed prior to the application of the dislocation-revealing etchant. One quadrant of the array was left undamaged to provide control diodes which have a relatively low dislocation density associated with threading dislocations from the CdZnTe substrate. Using x-ray Laue back-reflection measurements, the dislocations caused by the indentation were found to lie on {111} slip planes as seen in other previous work.[19]

The array was In-bump hybridized to a fanout and the I–V characteristics at zero field-of-view (FOV) were measured at 120, 78, and 40 K to obtain an initial assessment of the temperature dependence of any effects. Selected diodes were then characterized for R_0A versus temperature, spectral response, quantum efficiency, and $1/f$ noise. Upon completion of testing, the hybrid was pulled apart and the In-bumps, contact metallization, and the passivation layer were etched away. The HgCdTe (111)A top surface was etched using a recently reported defect etchant.[20] This etchant was found to give sharp triangular etch pits, as shown in the micrograph in Fig. 1, which are easy to distinguish from possible etching artifacts. The etch-pit density (EPD) for each diode was determined by dividing the number of etch pits on top of the mesa by that same area (junction area, A_j). In the undamaged regions, the EPD was approximately 10^5 cm^{-2}; this is also a typical value of EPD for CdZnTe substrates and is the origin of the threading dislocations in the LPE-grown HgCdTe layers. By monitoring the undamaged regions, it was found that no additional dislocations were introduced by either hybridizing the array to the fanout or by pulling apart the hybrid.

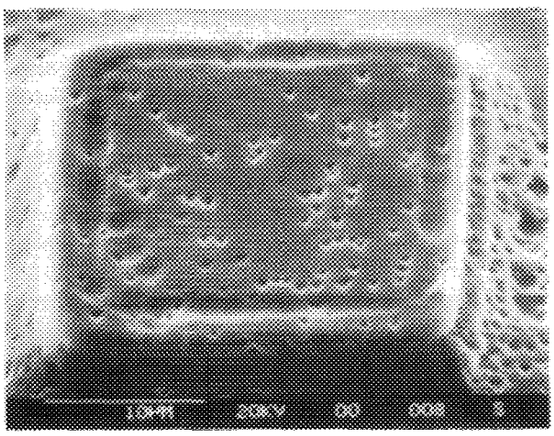

FIG. 1. Optical micrograph showing etch pits on HgCdTe (111)A surface.

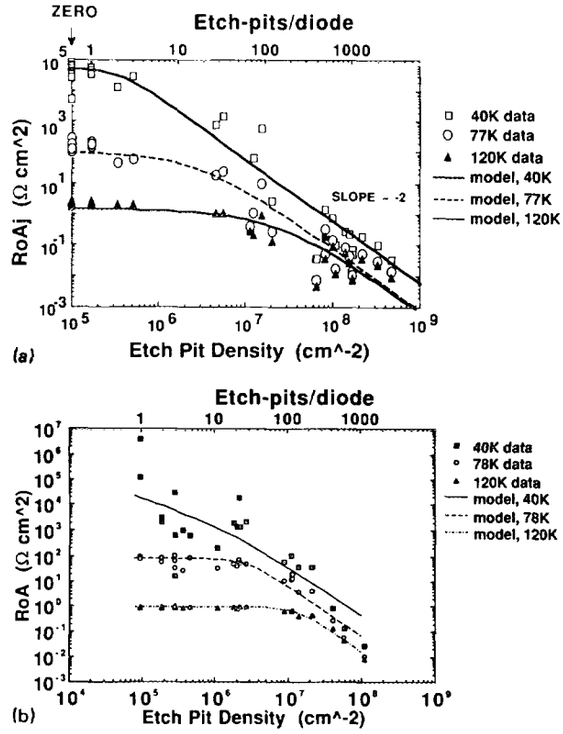

FIG. 2. R_0A_j vs EPD, showing fit of model to the data for (a) Array 1 and (b) Array 2, measured at 120, 78, and 40 K at zero FOV.

III. *I–V* CHARACTERISTICS

Figures 2(a) and 2(b) show a plot of R_0A_j versus EPD for Array 1 and Array 2, respectively, measured at 120, 78, and 40 K at zero FOV; at a given EPD, there are three data points for each diode corresponding to the three different measurement temperatures. For Array 1 in Fig. 2(a), the data points plotted at an EPD of 1×10^5 cm^{-2} are actually diodes which contained zero etch pits, but are plotted here since zero cannot be shown on a logarithmic scale, and it is also an EPD that is typical of undamaged HgCdTe. For Array 2, in Fig. 2(b), all of the diodes had at least one etch pit. At each temperature the data were fit to a theoretical model which will be discussed in detail in Sec. VI.

Figure 2 shows that for large EPD, R_0A_j decreases as the square of the EPD; this square dependence begins to dominate at lower EPD as the temperature decreases. Additionally, the effect of dislocations on R_0A_j is much more dramatic as the temperature decreases. At 78 K, R_0A_j begins to decrease at an EPD of approximately 10^6 cm^{-2}, while at 40 K, R_0A_j is immediately affected by the presence of one or more dislocations in a diode. The scatter in the R_0A_j data at large EPD may be associated with the presence of an increased number of pairs of "interacting" dislocations being present in some of those diodes; these pairs are more effective in reducing the R_0A_j than individual dislocations as discussed in Sec. VI. The scatter in the R_0A_j data at a given EPD also decreases substantially as the measurement temperature increases and the diodes go

Downloaded 26 Sep 2013 to 128.220.8.15. Redistribution subject to AVS license or copyright; see http://avspublications.org/jvstb/about/rights_and_permissions

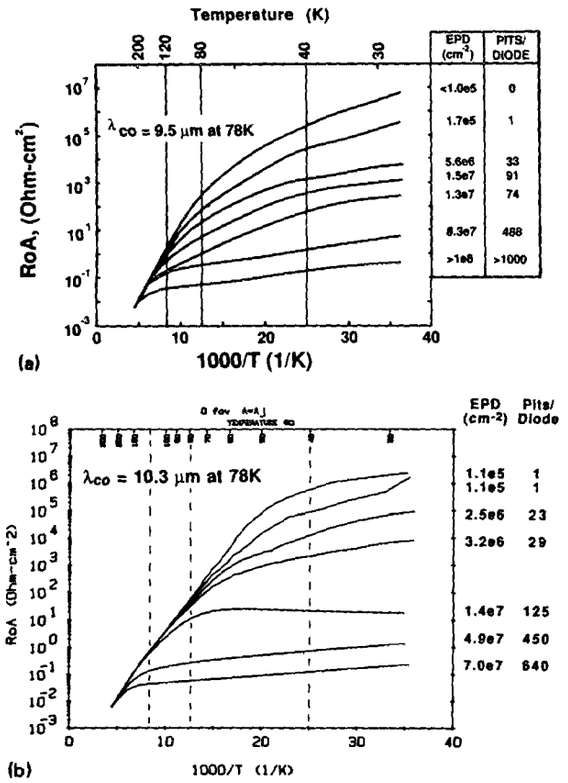

FIG. 3. R_0A_j vs $1/T$ measured at zero FOV for (a) Array 1 and (b) Array 2 showing the EPD for each diode.

from being limited by tunneling and g–r currents at lower temperatures to being dominated by diffusion currents at 120 K. Figure 2 clearly shows that high-quality (low EPD) materials are needed to achieve high-performance LWIR detectors operated at temperatures below 78 K.

In order to determine the mechanisms controlling the diode leakage currents, I–V characteristics were measured as a function of temperature at zero FOV for a sample of seven diodes from each array which covered the wide range in EPD. Figures 3(a) and 3(b) show a plot of R_0A_j versus $1/T$ for these diodes, for Array 1 and Array 2, respectively, and shows the EPD for each diode. At high temperatures all the diodes are diffusion limited and have about the same value of leakage current; thus it appears that the diffusion component of the leakage current is not strongly affected by dislocations. This was previously observed for intentionally damaged MWIR diodes[15] and for MWIR detectors co-fabricated on bulk CdZnTe and CdZnTe/GaAs/Si alternative substrates.[21] At 78 K, most of the diodes in Fig. 3(a) for Array 1 are g–r limited and show a much stronger increase in leakage current with increasing dislocation density. For Array 2, having a longer cutoff wavelength, shown in Fig. 3(b) many of the diodes are still diffusion limited at 78 K for EPD less than approximately 3×10^6 cm^{-2}. At 40 K and below, the diodes are tunneling limited for both arrays and an even larger spread in leakage current is seen as dislocation density increases.

Figure 4(a) shows, for Array 1, a plot of R_0A_j versus $1/T$ together with representative I–V characteristics at various temperatures for the best diode (zero etch pits), and Fig. 4(b) shows this same plot for diode with a dislocation density of 1×10^7 cm^{-2}. Figure 5 compares the R_0A_j verses $1/T$ for these same diodes and show a theoretical fit to the data. Both diodes have nearly the same diffusion current which varies as n_i^{-2}. In the g–r region, the best diode exhibits a classical n_i^{-1} slope proportional to $E_g/2$, as expected from theory, while the high dislocation density sample has a much smaller slope of $E_g/4$. This smaller slope may be g–r associated with multiple trap levels or possibly thermally activated trap assisted tunneling; further work is needed to understand this effect.

IV. SPECTRAL RESPONSE AND QUANTUM EFFICIENCY

The relative spectral response per photon of selected diodes from each array was measured at 78 K and is shown as a function of EPD in Figs. 6(a) and 6(b) for Array 1 and Array 2, respectively. Figure 6 shows that the relative response begins to decrease at shorter wavelengths as the EPD exceeds approximately 10^7 cm^{-2} for Array 1, shown in Fig. 6(a) and for an EPD of 5×10^7 cm^{-2} for Array 2 shown in Fig. 6(b). The results of Fig. 6 show that, unlike the R_0A_j product, the spectral response in these arrays is not very sensitive to dislocations until the dislocation density exceeds approximately 10^7 cm^{-2}. For backside-illuminated detectors, shorter wavelength photons will be generated closer to the substrate/layer interface and further from the p–n junction. Thus, the spectral response at shorter wavelengths is more sensitive to a decrease in the minority carrier diffusion length in the baselayer.

Figures 7(a) and 7(b) compare the relative spectral response measured at 120, 78, and 40 K for two diodes from Array 2 having an EPD of 1×10^5 cm^{-2} and an EPD of 5×10^7 cm^{-2}, respectively. Figure 7 shows that along with the cutoff wavelength increasing as the HgCdTe band gap decreases with lower temperature, the short wavelength spectral response decreases for the diode with the large EPD, shown in Fig. 7(b), which indicates that the minority carrier diffusion length is decreasing with temperature. This is probably due to increased Shockley–Read recombination associated with the dislocations.[15] For comparison there is no decrease in the short wavelength spectral response of the low EPD diode shown in Fig. 7(a).

The quantum efficiency of selected diodes from Array 1 was measured at 78 K using a spike filter at 8.3 μm; the quantum efficiency was calculated using the same assumed optical area of 1.3×10^{-5} cm^2 ($= 2A_j$) for each diode. The quantum efficiency for diodes from Array 2 was measured at 78 K using a spike filter at 4.0 μm; the quantum efficiency was calculated using the same assumed optical area of 2.5×10^{-5} cm^2 ($= 2.3A_j$) for each diode. The quantum efficiency of these diodes is shown as a function of EPD in Figs. 8(a) and 8(b) for Array 1 and Array 2,

Downloaded 26 Sep 2013 to 128.220.8.15. Redistribution subject to AVS license or copyright; see http://avspublications.org/jvstb/about/rights_and_permissions

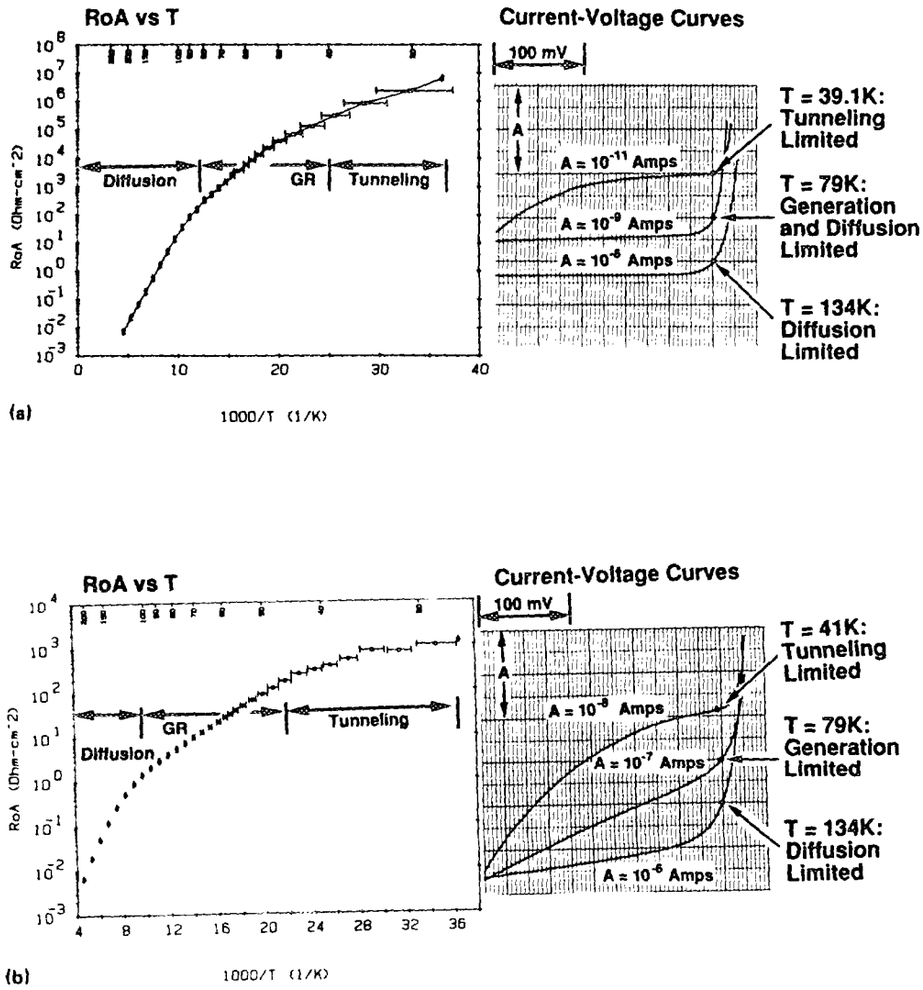

FIG. 4. R_0A_j vs $1/T$ for Array 1 with representative I–V characteristics at various temperatures for (a) the best diode (zero etch pits) and (b) a diode with a dislocation density of 1×10^7 cm^{-2}.

respectively. Figure 8 shows that, for both arrays, the quantum efficiency is only a weak function of EPD up to approximately 10^7 cm^{-2}. Thus, unlike the electrical properties of the detector (R_0A_j), the quantum efficiency and spectral response are not strongly affected by dislocations up to an EPD of approximately 10^7 cm^{-2}.

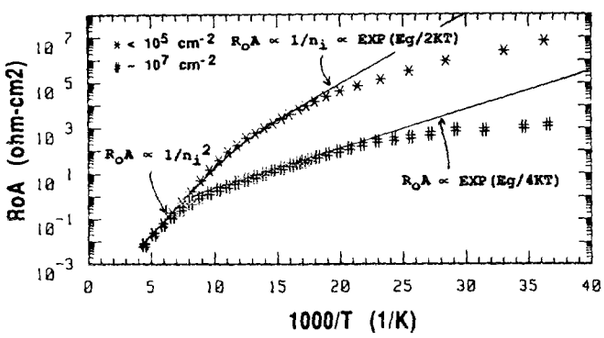

FIG. 5. R_0A_j vs $1/T$ for Array 1 showing the best diode (zero etch pits) and a diode with a dislocation density of 1×10^7 cm^{-2} with a theoretical fit to the data.

We have tried using an effective diffusion length model[22] to explain the variation of short-circuit current with dislocation density. In this model the effective minority carrier diffusion length L_{eff} is reduced by recombination at dislocations and is described by

$$\frac{1}{L_{\text{eff}}^2} = \frac{1}{L_0^2} + \frac{1}{L_{\text{dis}}^2}, \tag{1}$$

$$\frac{1}{L_{\text{dis}}^2} = \frac{\pi^3 N_{\text{dis}}}{4}, \tag{2}$$

where N_{dis} is the dislocation density and L_0 is the minority carrier diffusion length when dislocations are not present. The effective diffusion length was calculated as a function of dislocation density and then used as an input to another model to calculate the short-circuit current and open-circuit voltage of a HgCdTe p-on-n diode.

Downloaded 26 Sep 2013 to 128.220.8.15. Redistribution subject to AVS license or copyright; see http://avspublications.org/jvstb/about/rights_and_permissions

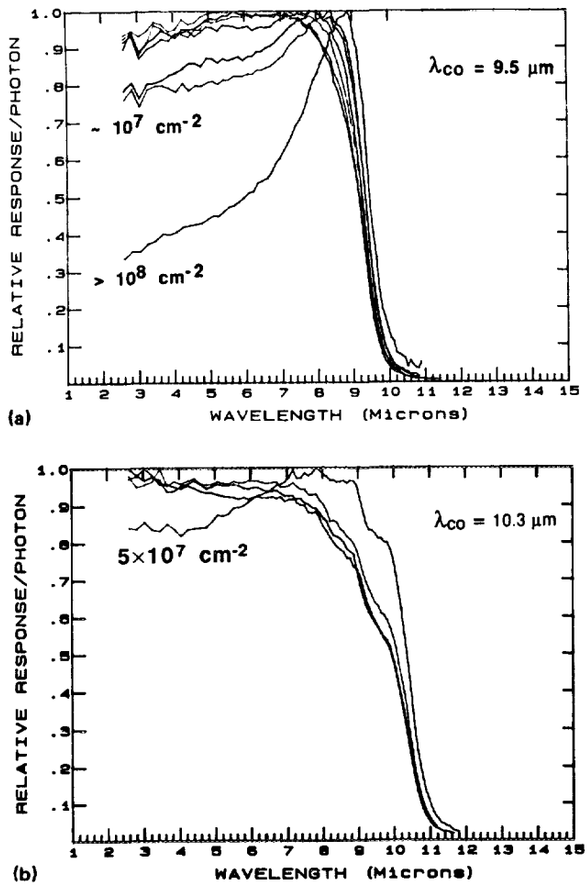

FIG. 6. Relative spectral response per photon vs wavelength measured at 78 K for selected diodes from (a) Array 1 and (b) Array 2 for various EPD.

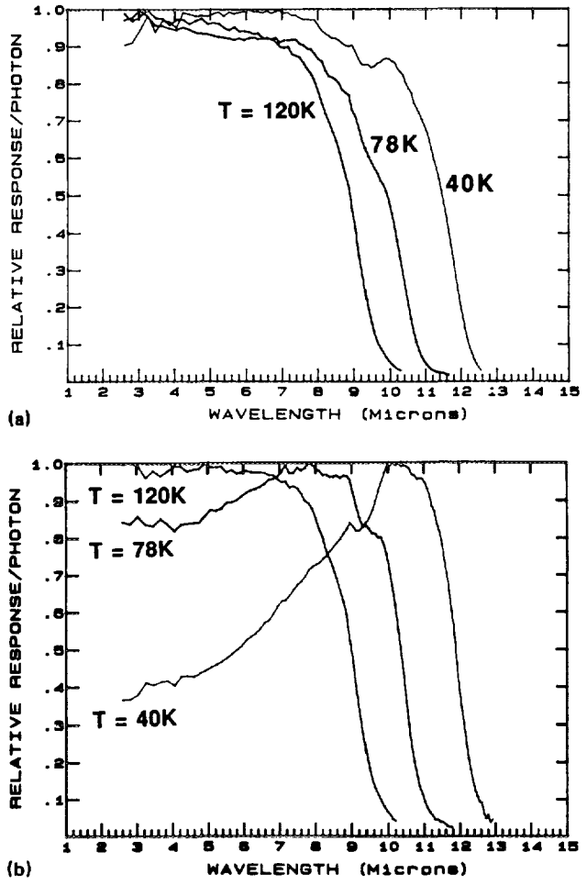

FIG. 7. Relative spectral response measured at 120, 78, and 40 K for two diodes from Array 2 having (a) an EPD of 1×10^5 cm^{-2} and (b) an EPD of 5×10^7 cm^{-2}.

Figure 9 shows a plot of the 78 K short-circuit current density at $f/2$ FOV versus dislocation density for the model calculation and experimental data points measured on Array 1. While the model shows a strong variation in short-circuit current with dislocation density, the experimental data show a weak dependence, similar to the quantum efficiency. This discrepancy may be a result of compositional grading in these LPE-grown HgCdTe diodes, which was not included in the model. The compositional grading in the baselayer of the detector gives rise to an electric field which forces minority carriers toward the junction and improves the collection efficiency and short-circuit current. Thus, the compositional grading in these detectors may be beneficial in reducing the magnitude of the effect that dislocations have on the spectral response and quantum efficiency.

V. 1/f NOISE

Noise measurements were made as a function of frequency at zero FOV, 78 K, and at a diode reverse bias of -20 mV for selected diodes in Array 1 and at $f/2$ FOV, 78 K, and at a diode reverse bias of -20 mV for selected diodes in Array 2. Figures 10(a) and 10(b) show a plot of the $1/f$ noise current at 1 Hz as a function of EPD for Array 1 and Array 2, respectively. Figure 10(a) shows that the noise current for Array 1 measured at zero FOV varies nearly linearly with EPD. Figure 10(b) shows that, for low EPD, the noise current is dominated by the photocurrent, while for higher EPD the noise current again varies nearly linearly with EPD.

Figure 11 shows the same $1/f$ noise currents from both arrays in Fig. 10 plotted instead as a function of the total diode current I_L. The $1/f$ noise current varies in a similar fashion to the fit of our historical database taken on undamaged diodes which varies as $I_L^{0.76}$. Thus, it appears that dislocations are not the direct source of $1/f$ noise, but rather increase it only through their effect on the leakage current. A similar variation in $1/f$ noise current was recently reported for leakage currents which were varied by changes in temperature, bias voltage, and electron irradiation damage.[23]

VI. MODEL DESCRIBING R_0A VERSUS DISLOCATION DENSITY

Figure 12(a) is a schematic of a cross section of a p-on-n mesa diode showing threading dislocations which intersect the junction and terminate on the mesa surface; with the use of a defect etch, each dislocation will be delineated

Downloaded 26 Sep 2013 to 128.220.8.15. Redistribution subject to AVS license or copyright; see http://avspublications.org/jvstb/about/rights_and_permissions

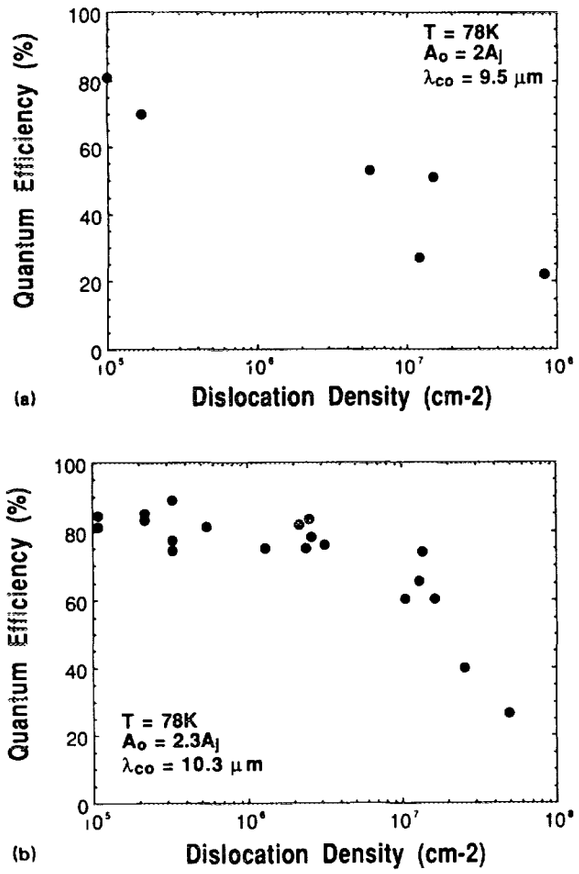

FIG. 8. Quantum efficiency vs dislocation density measured at 78 K for (a) Array 1 and (b) Array 2.

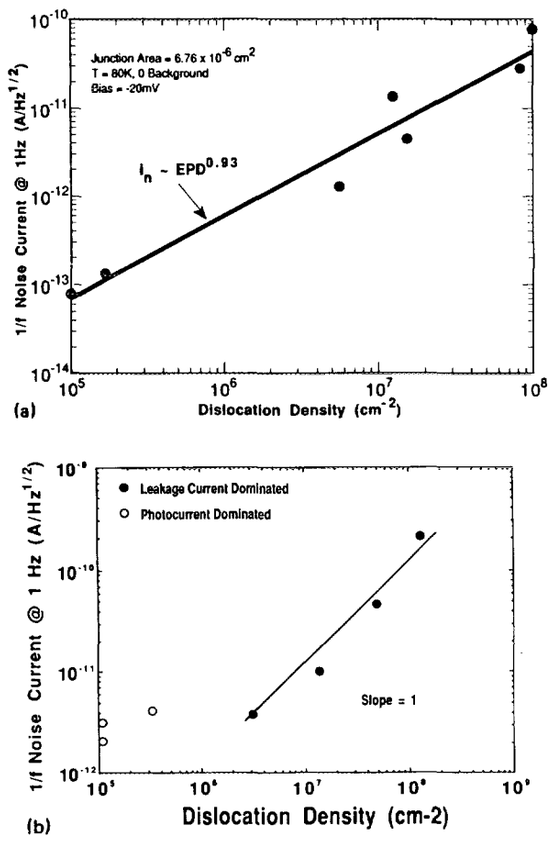

FIG. 10. $1/f$ noise current at 1 Hz vs dislocation density measured at 78 K for (a) Array 1 (zero FOV) and (2) Array 2 ($f/2$ FOV).

by a single etch pit at the surface of the mesa. Figure 12(b) shows an equivalent circuit of the mesa diode in Fig. 12(a). The conductance of the dislocation-free junction is g_0, each individual dislocation contributes a conductance g_1, and each pair of interacting dislocations contributes a conductance g_2. The conductance of an interacting pair is assumed to be greater than that of the sum of each individual dislocation ($g_2 > 2g_1$). The conductance of the junction is just the sum of the individual conductances of the dislocation-free junction, individual dislocations, and dislocation pairs. The R_0A product is then given by

$$R_0A = \frac{A}{g_0 + g_1A\lambda + g_2\dfrac{Aa\lambda^2}{2}}, \tag{3}$$

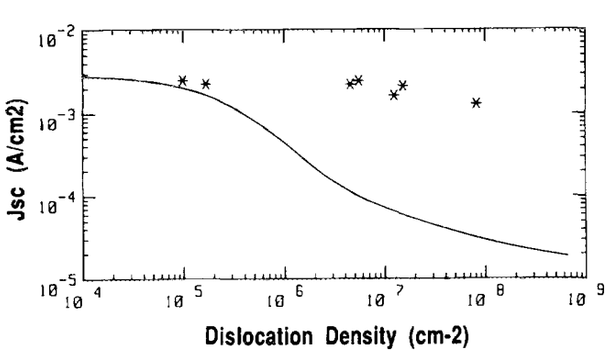

FIG. 9. Short-circuit current density at 78 K $f/2$ FOV vs dislocation density showing experimental data from Array 1 with a curve calculated using an effective diffusion length model.

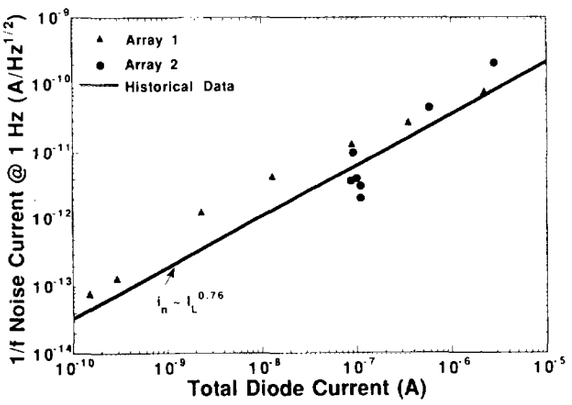

FIG. 11. $1/f$ noise current at 1 Hz vs total diode current for Array 1 and Array 2 at 78 K compared with fit to historical data on undamaged diodes.

Downloaded 26 Sep 2013 to 128.220.8.15. Redistribution subject to AVS license or copyright; see http://avspublications.org/jvstb/about/rights_and_permissions

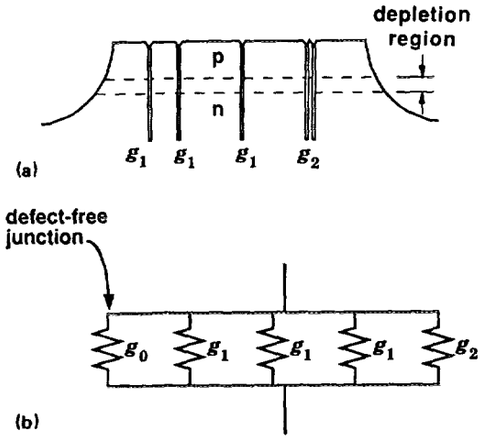

FIG. 12. (a) Schematic of a cross section of a *p*-on-*n* mesa diode showing threading dislocations which intersect the junction and terminate on the mesa surface, and (b) shows an equivalent circuit of the mesa diode in (a).

λ = dislocation density (cm^{-2}) = EPD; g_0 = conductance of dislocation-free junction; g_1 = conductance of isolated dislocation; g_2 = conductance of a pair of interacting dislocations; A = junction area; and a = pair interaction area. A pair of dislocations is assumed to interact if both lie within the interaction area a. It is expected that $a \ll A$. In Eq. (3) $A\lambda$ = average number of individual dislocations and $Aa\lambda^2/2$ = average number of interacting pairs of dislocations within a diode with junction area = A. The average number of interacting pairs is derived from the Poisson distribution as follows:

$$P_n(a) = \frac{(\lambda a)^n \exp(-\lambda a)}{n!}. \tag{4}$$

$P_n(a)$ is the Poisson distribution describing the probability of finding n defects with an area = a. The number of pairs out of n objects is $n(n-1)/2$. The average number of pairs of interacting dislocations in an area = A is given by

$$K = \frac{A}{a} \sum_{n=2}^{\infty} \frac{n(n-1)}{2} P_n(a). \tag{5}$$

Substituting $P_n(a)$ from Eq. (4) into Eq. (5) and after some algebra this reduces to $K = Aa\lambda^2/2$.

Thus using Poisson statistics and the assumption that closely spaced interacting pairs of dislocations have a higher conductance than two individual dislocations, leads to an expression for the diode R_0A product that varies with the square of the dislocation density as observed experimentally for large dislocation densities. Equation (3) was used to fit the experimental data taken at 120, 78, and 40 K and is shown in Figs. 2(a) and 2(b) to give a reasonable fit to the data. The conductances g_0, g_1, and g_2 determined from this fit, are shown plotted as a function of inverse temperature in Figs. 13(a) and 13(b) for Array 1 and Array 2, respectively. Although it cannot be uniquely determined from the model, the conductance g_2 was calculated from the g_2a product by assuming a dislocation interaction area of $a = 1\ \mu m^2$.

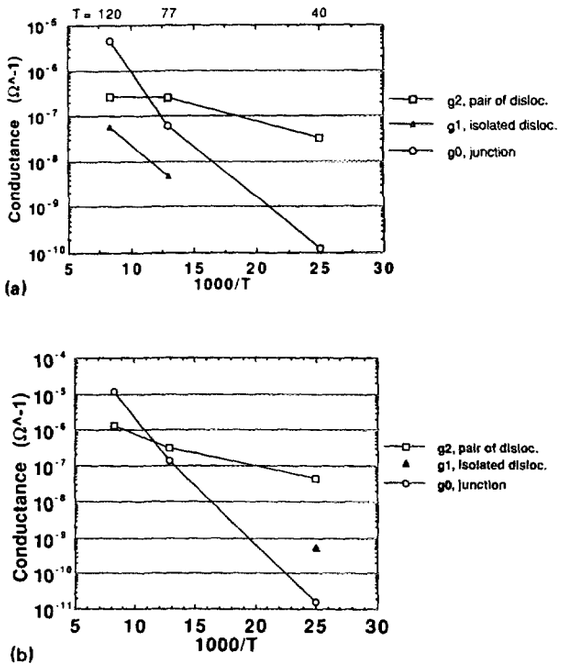

FIG. 13. Conductances for the defect-free junction (g_0), individual dislocation (g_1), and dislocation pair (g_2) determined from the model as a function of inverse temperature for (a) Array 1 and (b) Array (2).

Figure 13 shows that the conductance g_0 of the dislocation-free junction varies strongly with temperature and as approximately $Eg/2$ as expected for a LWIR HgCdTe diode. The conductance g_2 of a pair of interacting dislocations has a relatively weak temperature dependence and varies by about only an order of magnitude over the entire temperature range. The temperature dependence of the conductance g_1 of an isolated dislocation is apparently also weak, however, at some temperatures the fit of the experimental data to Eq. (3) was insensitive to the value used for g_1.

The physical mechanisms responsible for leakage associated with dislocations and dislocation pairs are not yet known and needs to be determined. We can speculate that the increased conductance associated with dislocation pairs may be caused by the physical intersection of two dislocations or possible caused by the overlap of a space-charge region associated with each dislocation. Clearly, more experimental and theoretical work is needed to understand these effects.

A related model of defect distributions, also based on Poisson statistics, has been developed to predict the R_0A distribution of a large area array of diodes.[24] This model can be used in conjunction with Eq. (3) to predict the R_0A distribution as a function of temperature and dislocation density. This allows an extremely useful analysis to be made of the effect of dislocations on overall array performance, uniformity, and operability.

VII. SUMMARY AND CONCLUSIONS

Dislocations originating from material growth and array processing can affect the overall performance, unifor-

Downloaded 26 Sep 2013 to 128.220.8.15. Redistribution subject to AVS license or copyright; see http://avspublications.org/jvstb/about/rights_and_permissions

mity, and operability of HgCdTe IRFPAs. To determine quantitatively their effect, dislocations were deliberately introduced by indentation into localized regions of LWIR HgCdTe arrays, device characteristics were measured, and the arrays were then preferentially etched to reveal the dislocations on each diode. Results show that dislocations can have a dramatic effect on the device characteristics of PV LWIR HgCdTe detectors, particularly at temperatures below 78 K. For large dislocation densities, R_0A decreases as the square of the dislocation density; the onset of this square dependence occurs at progressively lower dislocation densities as the temperature decreases. A phenomenological model was developed which describes the dependence of the detector R_0A product with dislocation density, based on the conductances of individual and interacting dislocations which shunt the p–n junction; this model was found to give a reasonable fit to the experimental data. The physical mechanisms responsible for leakage associated with dislocations and dislocation pairs are not yet known and further work is needed to understand these processes.

The temperature dependence of R_0A for high dislocation densities shows a g–r slope close to $E_g/4$, rather than $E_g/2$ as expected from theory which may be associated with multiple trap levels. Spectral response and quantum efficiency are only weakly affected, as is the diffusion component of the leakage current. A model based on an effective diffusion length varying with dislocation density failed to fit the experimental data of short-circuit current versus dislocation density. This discrepancy may be a result of compositional grading in these LPE-grown HgCdTe diodes which improves the collection efficiency and short-circuit current. The $1/f$ noise current was found to increase approximately linearly with dislocation density. The $1/f$ noise current also tracks with the magnitude of the leakage current, similar to the behavior of our historical data trendline established for undamaged HgCdTe devices.

The results of this study can be used to understand the performance limitations of LWIR HgCdTe arrays fabricated on heteroepitaxial substrates. We have already demonstrated 78 K high-performance LWIR 128×128 arrays,[25] and more recently, 256×256, and 480×640 arrays of HgCdTe grown by LPE on alternative substrates of CdZnTe/GaAs/Si. These heteroepitaxial materials, which have a dislocation density of approximately 10^6 cm^{-2}, have a performance that is entirely consistent with that expected from this study. Thus, these materials are suitable for fabricating high-performance large-area arrays for 78 K applications; a reduction in the dislocation density will be needed to achieve higher performance for lower temperature applications.

ACKNOWLEDGMENTS

This work was funded by Naval Research Laboratories under Contract No. N00014-88-C-2468. The contract monitor is Dr. William A. Schmidt.

[1] H. Takigawa, T. Akamatsu, T. Kanno, and R. Tsunoda, *Proceedings of the IEDM Conference, 1981* (IEEE, New York, 1981), p. 172.
[2] A. J. Syllaios and L. Columbo, *Proceedings of the IEDM Conference, 1982* (IEEE, New York, 1982), p. 137.
[3] H. F. Schaake and A. J. Lewis, in *Defects in Semiconductors*, Materials Research Society Symposium Proceedings, edited by S. Mahajan and J. W. Corbett (Elsevier, New York, 1983), Vol. 14, p. 301.
[4] L. Columbo and A. J. Syllaios, *Proceedings of the IEDM Conference, 1983* (IEEE, New York, 1983), p. 718.
[5] H. F. Schaake, J. H. Tregilgas, A. J. Lewis, and P. M. Everett, J. Vac. Sci. Technol. A **1**, 1625 (1983).
[6] T. Yamamoto, Y. Miyamoto, and K. Tanikawa, J. Cryst. Growth **72**, 270 (1985).
[7] Y. Miyamoto, H. Sakai, and K. Tanikawa, Proc. SPIE, **572**, 115 (1985).
[8] J. H. Tregilgas, T. L. Polgreen, and M. C. Chen, J. Cryst. Growth **86**, 460 (1988).
[9] D. Chandra and M. W. Goodwin, in *Properties of II-VI Semiconductors: Bulk Crystals, Epitaxial Films, Quantum Well Structures, and Dilute Magnetic Systems*, Materials Research Society Symposium Proceedings, edited by F. J. Bartoli, Jr., H. F. Schaake, and J. F. Schetzina (Materials Research Society, Pittsburgh, PA, 1990), Vol. 161, p. 313.
[10] D. Chandra, J. H. Tregilgas, and M. W. Goodwin, J. Vac. Sci. Technol. B **9**, 1852 (1991).
[11] R. S. List, J. Vac. Sci. Technol. B **10**, 1651 (1992).
[12] S. G. Gasan-zade, E. A. Sal'kov, and G. A. Shepel'skii, Sov. Phys. Semicond. **17**, 1225 (1983).
[13] M. G. Andrukhiv, I. S. Virt, D. I. Tsyutsyura, D. S. Shuptar, and P. S. Shkumbatyuk, Sov. Phys. Semicond. **23**, 787 (1989).
[14] P. I. Baranskii, A. E. Belyaev, O. P. Gorodnichii, and S. M. Komirenko, Sov. Phys. Semicond. **24**, 73 (1990).
[15] S. H. Shin, J. M. Arias, D. D. Edwall, M. Zandian, J. G. Pasko, and R. E. DeWames, J. Vac. Sci. Technol. B **10**, 1492 (1992).
[16] P. W. Norton and A. P. Erwin, J. Vac. Sci. Technol. A **7**, 503 (1989).
[17] T. Tung, M. H. Kalisher, A. P. Stevens, and P. E. Herning, in *Materials for Infrared Detectors and Sources*, edited by R. F. C. Farrow, J. F. Schetzina, and J. T. Cheung (Materials Research Society Pittsburgh, PA, 1987), Vol. 90, p. 321.
[18] T. Tung, J. Cryst. Growth **86**, 161 (1988).
[19] M. Brown and A. F. W. Willoughby, J. Phys. C **6**, C6-151 (1979).
[20] I. Hähnert and M. Schenk, J. Cryst. Growth **101**, 251 (1990).
[21] S. M. Johnson, M. H. Kalisher, W. L. Ahlgren, J. B. James, and C. A. Cockrum, Appl. Phys. Lett. **56**, 946 (1990).
[22] J. C. Zolper and A. M. Barnett, IEEE Trans. Elect. Dev. **37**, 478 (1990).
[23] J. Bajaj, E. R. Blazejewski, G. M. Williams, R. E. DeWames, and M. Brown, J. Vac. Sci. Technol. B **10**, 1617 (1992).
[24] D. R. Rhiger, R. D. Rodriguez, and J. M. Peterson, Proc. 1991 IRIS Detector Specialty Conference (in press).
[25] S. M. Johnson, J. B. James, W. L. Ahlgren, W. J. Hamilton, Jr., M. Ray, and G. S. Tompa, in *Long-Wavelength Semiconductor Devices, Materials, and Processes*, Materials Research Society Symposium Proceedings, edited by A. Katz, R. M. Biefeld, R. L. Gunshor, and R. J. Malik (Materials Research Society, Pittsburgh, PA, 1991), Vol. 216, p. 141.

Downloaded 26 Sep 2013 to 128.220.8.15. Redistribution subject to AVS license or copyright; see http://avspublications.org/jvstb/about/rights_and_permissions